J Toxicol Pathol 2024; 37: 189–195

Case Report

Spontaneous B-cell lymphoma in the cranial mediastinal lymph node of an aged male C57BL/6J mouse

Shoko Suzuki[1*], Mao Mizukawa[1], Akane Kashimura[1], Hironobu Nishina[1], Tetsuya Sakairi[1], and Satomi Nishikawa[1]

[1] Safety Research Laboratories, Research Division, Mitsubishi Tanabe Pharma Corporation, 2-26-1 Muraoka-Higashi, Fujisawa-shi, Kanagawa 251-8555, Japan

Abstract: B-cell lymphoma is generally observed in the spleen, mesenteric lymph nodes, and Peyer's patches in aged mice and rarely appears in other organs. Herein, we report a case of spontaneous B-cell lymphoma originating from the cranial mediastinal lymph node in a male 75-week-old C57BL/6J mouse. Macroscopically, a white mass was found at the base of the heart with no connection to the thymus. Microscopic examination revealed a solid proliferation of tumor cells with large nuclei at the center of the mass. Some macrophages, normal-sized lymphocytes, and lymphatic sinuses were found in both central and peripheral areas. Immunohistochemical analysis showed positive staining for cluster of differentiation 19, paired box protein 5, immunoglobulin M, and Ki-67 but not for cytokeratin AE1/AE3. These findings were not completely consistent with the established mouse lymphoma classification, leading to a diagnosis of B-cell lymphoma originating from the cranial mediastinal lymph node. This case report is the first to document a B-cell lymphoma in the cranial mediastinal lymph nodes in an aged C57BL/6J mouse. (DOI: 10.1293/tox.2023-0130; J Toxicol Pathol 2024; 37: 189–195)

Key words: B-cell lymphoma, cranial mediastinal lymph node, spontaneous lesion, C57BL/6J mouse

Lymphomas are common, spontaneously occurring tumors in mice. Most mouse lymphomas are age related and have been reported in CD-1, B6/129, and C57BL/6 strains[1–3]. The classification of mouse lymphomas has been used by pathologists for over 80 years[4–7]. In the 2000s, the World Health Organization (WHO)[8] and the Mouse Models of Human Cancers Consortium (MMHCC)[9] developed a mouse lymphoma classification system. Meanwhile, the International Harmonization of Nomenclature and Diagnostic Criteria (INHAND) classification of mouse lymphomas was published in 2019[10]. In those classification systems, subclassifications were also reported based on morphological features and cell origin (e.g., B- or T-cell origin). B-cell lymphomas in mice typically occur in the spleen, mesenteric lymph node, and Peyer's patches, with occurrences in other organs being rare[10, 11, 15]. In this report, we describe a case of spontaneous B-cell lymphoma arising in the cranial mediastinal lymph node of an aged C57BL/6J mouse.

A male C57BL/6J mouse (74 weeks old) were purchased from Jackson Laboratory Japan, Inc. (formerly Charles River Laboratories Japan Inc., Atsugi, Japan). They had free access to food (autoclaved CRF-1; Oriental Yeast Co., Ltd., Tokyo, Japan) and tap water. After a 1-week quarantine and acclimation period, the mouse was sacrificed at 75 weeks of age. No clinical signs were observed until treatment termination. At termination, the mouse was euthanized by exsanguination, which was induced by immediately cutting the abdominal aorta under deep isoflurane anesthesia. The external body surface, thoracic and abdominal cavities, and viscera were examined macroscopically. At necropsy, a white mass was observed on the base of the heart. The border between the white mass and based of the heart was clear (Fig. 1A and 1B), and the mass was excised along with the heart. Thymic involution was also observed, with no connection between the mass and thymus. No significant lesions were observed in the other organs. Hematological, blood chemistry, and organ weight measurements were not performed. All procedures were carried out in accordance with the animal welfare guidelines and Rules for Feeding and Storage of Experimental Animals and Animal Experiments of Mitsubishi Tanabe Pharma Corporation.

All the organs and tissues, including the white mass, were collected and fixed in 10% neutral-buffered formalin for histopathological examination. The tissues were dehydrated and embedded in paraffin. The paraffin-embedded sections (4 μm thick) were stained with hematoxylin and eosin (H&E). The white mass was further examined using im-

Received: 17 December 2023, Accepted: 12 June 2024
Published online in J-STAGE: 3 July 2024
*Corresponding author: S Suzuki
(e-mail: suzuki.shoko@ma.mt-pharma.co.jp)

munohistochemical staining for the detection of cluster of differentiation (CD) 19, paired box protein 5 (PAX5), immunoglobulin M (IgM), CD3, ionized calcium-binding adapter molecule 1 (Iba-1), Ki-67, and cytokeratin (CK) AE1/AE3. Details of the primary antibodies (incubation time and temperature), antigen retrieval methods, secondary antibodies, and detection of positive signals are summarized in Table 1. All sections were counterstained with hematoxylin. In addition, the mass was examined by performing a double immunohistochemical staining for Ki-67 and CD19. The primary antibodies, secondary antibodies, and antigen retrieval conditions for Ki-67 and CD19, as well as the conditions for blocking endogenous peroxidase activity and nonspecific staining for Ki-67, were the same as those used for single staining. Following the same procedure as that used for single Ki-67 staining, the sections were heated for antigen retrieval, incubated with an anti-CD19 antibody overnight at 4°C, and incubated with the secondary antibody for 30 min at room temperature. HistoGreen Substrate Kit for peroxidase (E109, Cosmo Bio Co., Ltd., Tokyo, Japan) was used to detect the presence of CD19 in the sections after counterstaining with hematoxylin.

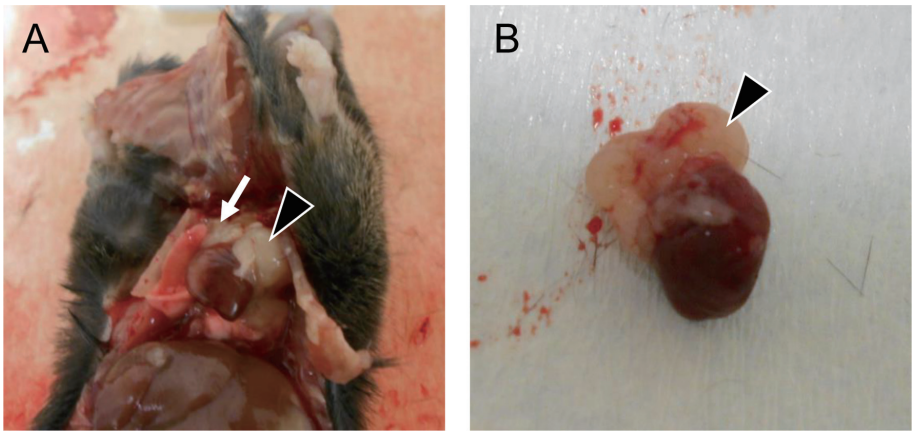

Fig. 1. Gross appearance in the thoracic cavity. (A) A large white mass within the mediastinum (arrowhead) and involutional thymus (arrow). (B) The mass was located in the base of the heart (arrowhead).

Table 1. Primary Antibodies Used for Immunohistochemistry

Antibody target	Host species	Clonality	Clone	Dilution Incubation time Temperature	Supplier	Antigen retrieval method	Blocking	Secondary antibody*	Detection of positive signals
Ki-67	Rat	Monoclonal	SolA15	1:100 1 hour, RT	eBioscience™, Tokyo, Japan	HIER, Citrate pH 6.0†, 20 min	3% H_2O_2: 10 min, Block Ace‡: 30 min, RT	Histofine Simple Stain Mouse MAX-PO§, Rat, 30 min, RT	Erythroid and myeloid cells in spleen
CD19	Rabbit	Monoclonal	EPR23174-145	1:1000 1 hour, RT	Abcam, Cambridge, UK	HIER, Tris/EDTA pH 9.0¶, 20 min	3% H_2O_2: 10 min, Block Ace: 30 min, RT	Histofine Simple Stain Mouse MAX-PO, Rabbit, 30 min, RT	Lymphoid follicle in spleen
PAX5	Rabbit	Monoclonal	EPR3730(2)	1:1000 1 hour RT	Abcam, Cambridge, UK	HIER, Tris/EDTA pH 9.0, 20 min	3% H_2O_2: 10 min, Block Ace: 30 min, RT	Histofine Simple Stain Mouse MAX-PO, Rabbit, 30 min, RT	Lymphoid follicle in spleen
IgM	Goat	Polyclonal	μ-chain	1:400 1 hour RT	Jacson ImmunoResearch Inc., PA, USA	HIER, Citrate pH 6.0, 20 min	3% H_2O_2: 10 min, Block Ace: 30 min, RT	Histofine Simple Stain Mouse MAX-PO, Goat, 30 min, RT	Mott cells in the surrounding tissue of the mass
CD3	Rabbit	Monoclonal	SP7	Ready to use 1 hour RT	Nichirei Biosciences, Tokyo, Japan	HIER, Citrate pH 6.0, 20 min	3% H_2O_2: 10 min, Block Ace: 30 min, RT	Histofine Simple Stain Mouse MAX-PO, Rabbit, 30 min, RT	Periarterial lymphoid sheath (PALS) in spleen
Iba-1	Rabbit	Polyclonal	-	1:5000 1 hour RT	Fujifilm Wako Chemicals, Osaka, Japan	HIER, Citrate pH 6.0, 20 min	3% H_2O_2: 10 min, Block Ace: 30 min, RT	Histofine Simple Stain Mouse MAX-PO, Rabbit, 30 min, RT	Macrophages in spleen
CK	Mouse	Monoclonal	AE1/AE3	Ready to use 1 hour RT	Nichirei Biosciences, Tokyo, Japan	HIER, Citrate pH 6.0, 20 min	3% H_2O_2: 10 min, Histofine Mouse Stain Kit‡: following the manufacturer's protocol	Histofine Simple Stain Mouse MAX-PO, Mouse, 30 min, RT	Thymic Epithelial cells

*: Positive reactions were visualized with a Peroxidase Stain DAB Kit (Nacalai Tesque Inc., Kyoto, Japan), †: LSI Medience Co., Ltd., ‡: DS Pharma Biomedical Co., Ltd., §: Nichirei Bioscience Inc., ¶: DAKO [Agilent Technologies, Ltd.], ⁑: Nichirei Bioscience Inc. HIER: Heat-Induced Epitope Retrieval; RT: Room temperature.

Microscopically, the mass consisted of two small masses and one large mass, which were demarcated from the heart by the surrounding fibrous or fatty tissue (Fig. 2). In each mass, the tumor cells exhibited scant to moderate basophilic cytoplasm, large round to oval nuclei, and 1–3 prominent nucleoli that proliferated solidly in the center (Fig. 3A, small mass). Occasional single-cell necrosis and mitotic figures were noted (1–2 mitoses per high-power field). Tingible-body macrophages were rarely observed. In addition to tumor cells, each mass contained mixtures of large cells and normal lymphocytes. In the periphery of small masses, the areas of normal-sized lymphocytes were compressed by tumor cells (Fig. 3B). Normal-sized lymphocytes were more prevalent in the large mass than in the small masses (Fig. 3C), and peripheral lymphatic sinuses filled with normal-sized lymphocytes were observed (Fig. 3D). Normal-sized lymphocytes, plasma cells, and mott cells were noted in the surrounding tissues (Fig. 3E). In the left heart atrium adjacent to the mass, mineralization and macrophages with brown pigment were observed (Fig. 3F). No related findings were noted in other organs.

Immunohistochemical staining results are presented in Table 2. Ki-67 was mainly expressed in tumor cells at the center of each mass and rarely in normal-sized lymphocytes throughout each mass. Large cells in the masses and normal-sized lymphocytes in the surrounding tissues were negative for Ki-67 (Fig. 4A). CD19 was expressed in the tumor cells at the center of each mass and in some normal-sized lymphocytes throughout each mass and the surrounding tissue, but not in large cells within each mass (Fig. 4B). The expression pattern of PAX5 was similar to that of CD19. IgM was weakly expressed in some tumor cells throughout each mass and strongly expressed in some normal-sized lymphocytes in each mass and the surrounding tissue, but not in large cells (Fig. 4C). CD3 was expressed in some normal-sized lymphocytes throughout each mass and the surrounding tissues, but not in tumor cells or large cells in each mass (Fig. 4D). Iba-1 was expressed in large cells throughout each mass (approximately 50% of large cells) but not in the tumor cells or normal-sized lymphocytes in each mass or the surrounding tissue (Fig. 4E). CK AE1/AE3 was not expressed in any of the observed masses (Fig. 4F). Double immunohistochemical staining showed that Ki-67 and CD19 were co-expressed in tumor cells at the center of each mass (Fig. 4G). However, only CD19 was expressed in normal lymphocytes and cells in the lymphatic sinus on the periphery of each mass (Fig. 4H).

Based on the above histological findings, the case was diagnosed with B-cell lymphoma of the cranial mediastinal lymph node that spontaneously occurred in an aged male mouse. We concluded that the lymphoma originated from the lymph node owing to the presence of lymphatic sinus in the mass, the absence of CK AE1/AE3 expression in each mass, and the absence of connection to the thymus. Most normal-sized lymphocytes in the tumors did not express Ki-67. This result indicated that the normal-sized lymphocytes in each mass were normal. The Iba-1-positive large cells in the masses, which were considered reticular cells or macrophages, increased or infiltrated in response to the presence of tumor cells and single-cell necrosis. The mineralization and infiltration of pigmented macrophages in the left heart atrium were presumed to be secondary changes related to mass compression.

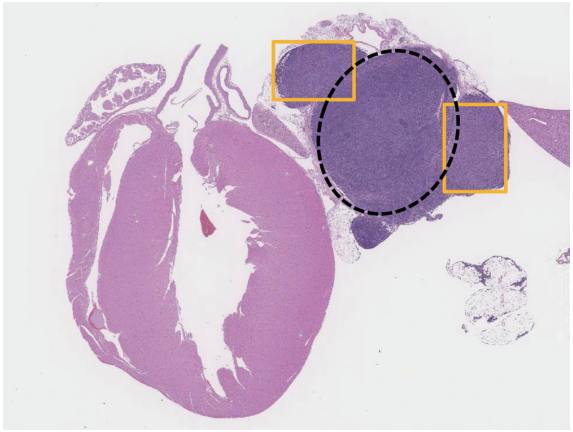

Fig. 2. H&E staining of the mass along with the heart. The mass consisted of two small masses (yellow boxed area) and one large mass (black dotted round area). They were clearly demarcated from the heart by the surrounding tissue.

The classification of mouse lymphomas based on histological characteristics was published by Dunn in 1954[4]. Subsequent classifications were established following the identification of T- and B-cell lymphocyte subsets in the 1970s, including Pattengale and Taylor's classification in 1983[5] and Fredrickson's classification in 1994[7]; these classifications adopted the human classifications of Lukes-Collins and Kiel, respectively. In 2001, the WHO mouse classification was proposed by a committee of international pathologists[8]. This WHO mouse classification was regarded as the most useful classification when developing safety assessment studies. In 2002, a comprehensive tumor classification for humans and genetically engineered mice was proposed by the MMHCC of the National Cancer Institute[9] based on the WHO human hematopoietic tumor classification. The MMHCC classification is useful for the assessment of humans and genetically engineered mice, but not for toxicology studies. In 2019, a classification of rat and mouse lymphomas (non-proliferative and proliferative lesions of the rat and mouse hematolymphoid systems)[10] was published based on the INHAND Project. This project was established in 2008 to provide a standardized nomenclature for microscopic lesions in laboratory rats and mice. The INHAND classification is commonly used to classify toxicological pathologies.

We applied the INHAND, WHO, and MMHCC classifications based on the case of our case. The modifiers for lymphoma in the INHAND classification, which are used to sub-classify lesions, are summarized in Table 3. The current case exhibited morphological features, including the solid proliferation of tumor cells with large round to oval

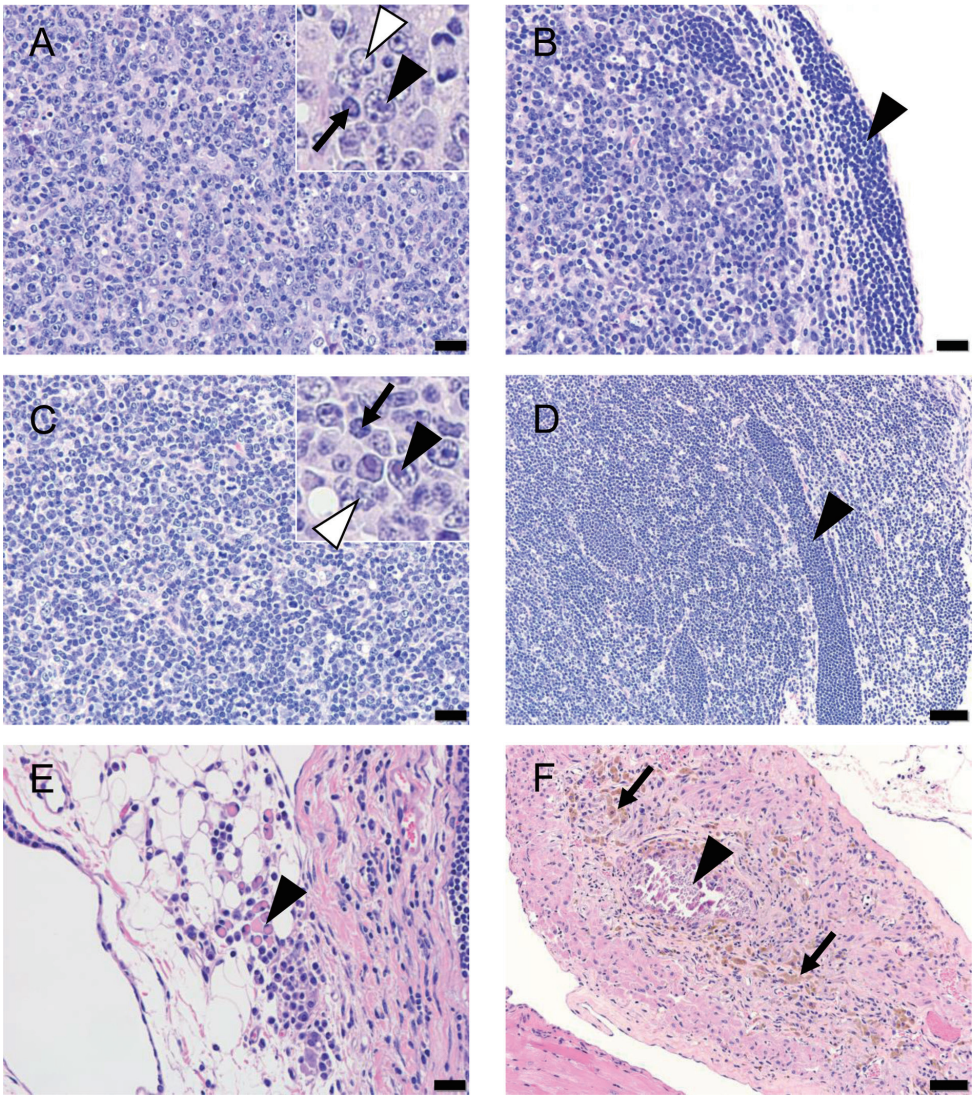

Fig. 3. H&E staining of the mass. (A) The center of the small mass, composed mainly of tumor cells (inset: tumor cells [black arrowhead], large cells [white arrowhead], and normal-sized lymphocytes [arrow]). Bar=20 µm. (B) The periphery of the small mass, composed mainly of normal-sized lymphocytes (arrowhead). The areas of normal-sized lymphocytes were compressed by the tumor cells. Bar=20 µm. (C) The center of the large mass, composed mainly of tumor cells (inset: tumor cells [black arrowhead], large cells [white arrowhead], and normal-sized lymphocytes [arrow]). Bar=20 µm. (D) The periphery of the large mass, composed mainly of normal-sized lymphocytes and lymphatic sinus (arrowhead). Bar=50 µm. (E) The tumor-surrounding tissue. Mott cells (arrowhead) were sporadically observed. Bar=20 µm. (F) The left heart atrium. Mineralization (arrowhead) and macrophages with brown pigment (arrow) were observed. Bar=20 µm.

Table 2. Results of Immunohistochemistry

Antibody	Small masses			Large mass			Surrounding tissue
	Tumor cells	Large cells	Normal sized lymphocytes	Tumor cells	Large cells	Normal sized lymphocytes	Normal sized lymphocytes
Ki-67	+	−	−/+	+	−	−/+	−
CD19	+	−	+*	+	−	+*	+*
PAX5	+	−	+*	+	−	+*	+*
IgM	+**	−	−/+	+**	−	−/+	+
CD3	−	−	+*	−	−	+*	+*
Iba-1	−	+	−	−	+	−	−
CK AE1/AE3	−	−	−	−	−	−	−

−: negative, +: positive, −/+: almost negative, *: positive for either CD19/PAX5 or CD3, **: weakly positive.

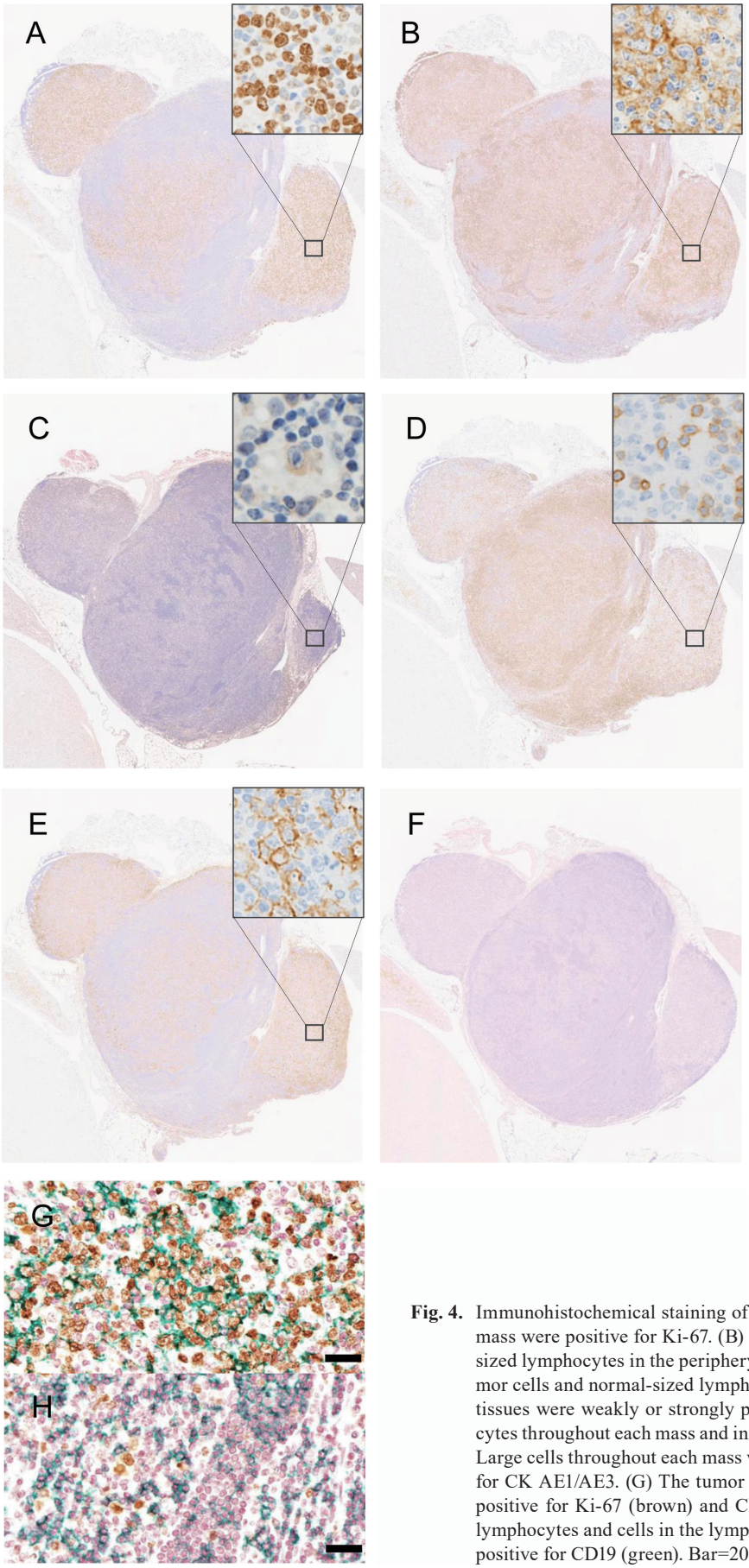

Fig. 4. Immunohistochemical staining of the mass. (A) The tumor cells at the center of the mass were positive for Ki-67. (B) Tumor cells at the center of the mass and normal-sized lymphocytes in the periphery of the mass were positive for CD19. (C) Some tumor cells and normal-sized lymphocytes throughout each mass and the surrounding tissues were weakly or strongly positive for IgM. (D) Some normal-sized lymphocytes throughout each mass and in the surrounding tissues were positive for CD3. (E) Large cells throughout each mass were positive for Iba-1. (F) All areas were negative for CK AE1/AE3. (G) The tumor cells in the center of the small mass were double positive for Ki-67 (brown) and CD19 (green). Bar=20 μm. (H) Most normal-sized lymphocytes and cells in the lymphatic sinus in the periphery of the large mass were positive for CD19 (green). Bar=20 μm.

Table 3. Modifiers to the Published International Harmonization of Nomenclature and Diagnostic Criteria (INHAND) Guideline

Lymphoma		Origin	Positive result of IHC
Subtype modifiers	Lymphoblastic lymphoma	B cells, T cells	B-cell origin: PAX5, CD45R (negative when cells are in the pro-B stage)
	Pleomorphic lymphoma	Follicular B cells, T cells (rare)	B-cell origin: heavy chain Igs and kappa light chains, lambda light chains (rare)
	Follicular lymphoma	B cells	CD45R/B220, PAX5, CD79a, BCL6, PNA
	Immunoblastic lymphoma	B cells, T cells (rare)	B-cell origin: heavy chain Igs or kappa light chains and lambda light chains (rare)
	Lymphocytic lymphoma	B cells, T cells	-
	Plasmacytic lymphoma	Plasma cells	Heavy chain Igs, kappa light chains
	Epitheliotropic cutaneous lymphoma	T cells	T-cell origin: CD2, CD3, CD8
	Marginal zone lymphoma	B cells	PAX5, CD45R, IgM
	Large granular lymphocyte leukemia	Large granular lymphocytes (NK cells)	OX-8 (CD8)
Cell type modifiers	T cell or B cell		
Qualifier (optional)	Leukemic can be used when there is an obvious leukemia present judging from the peripheral blood smears or tissue sections.		

IHC: Immunohistochemistry.

nuclei and scanty to moderate basophilic cytoplasm. These features have been noted in lymphoblastic lymphoma, pleomorphic lymphoma, follicular lymphoma, and immunoblastic lymphoma based on the INHAND subclassification of lymphoma. In lymphoblastic and immunoblastic lymphomas, monotypic proliferation of tumor cells is observed; therefore, it is different from the characteristics of current case, which exhibited admixtures of large cells (reticular cells or macrophages) and lymphocytes. Our current case is similar to pleomorphic lymphoma or follicular lymphoma because admixtures of several cell types are a characteristic of these tumors which are derived from follicles. In our case, neither follicular structures or pre-existing follicles were observed in each mass; however, these structures may have been indistinct because of the severe infiltration of tumor cells. However, our case could not be diagnosed with follicle-derived tumor as centrocytes (or centrocyte-like cells) were not clearly observed. Although we applied the WHO mouse classification[8], the morphological features of our current case were not completely consistent with this classification, echoing similar discrepancies found in the INHAND classification. Finally, we applied the MMHCC classification and found that the characteristics of our current case closely resembled those of histiocyte-associated diffuse large B-cell lymphoma (DLBCL)[9, 12]. Our case showed solid proliferation of tumor cells with large cells (reticular cells or macrophages) and lymphocytes, similar to the characteristics of histiocyte-associated DLBCL. This includes approximately 50% of large histiocytes (macrophages) admixed with centroblastic and immunoblastic B cells and variable numbers of smaller T cells. However, definitive diagnosis requires the analyses of immunophenotypic and genetic characteristics, which is hindered by the unavailability of the classification website. According to the MMHCC, DLBCL is predominantly observed in inbred strains and some genetically engineered mouse lines, while true DLBCL is rarely observed in aging CD-1 and B6C3F1 mice[9, 11]. As this classification has been proposed for human tumor models, the relationship between DLBCL and our current case remains unclear.

This case report revealed that the tumor cells were not of plasma cell origin owing to their PAX5 positivity[13]. Based on the INHAND classification, lymphomas originating from B cells cannot be clearly differentiated by immunohistochemical staining (Table 3). Various immunophenotypes of mouse lymphomas have been reported, but the subclassifications have not been standardized[9, 13–15].

Accordingly, our case was diagnosed with B-cell lymphoma. However, the characteristics of our current case closely resembles those of histiocyte-associated DLBCL within the abovementioned classifications. The MMHCC classification is intended for mouse models of human cancer; however, our case did not meet these criteria. Additionally, the morphological features of this case were not completely consistent with those stipulated in the INHAND and WHO subclassifications.

We suggest that the primary tumor site in our current case was the cranial mediastinal lymph node. Broeck *et al.* reported the positions of 22 lymph nodes in BALB/cAnNCrl mice[16]. According to their report, cranial mediastinal lymph nodes were located lateral to the thoracic thymus and along the internal thoracic artery and vein. Considering that the tumor in the current case was located at the base of the heart, the tumor may have originated from the cranial mediastinal lymph nodes or the thymus. Moreover, the mass was independent of the thymus and negative for CK AE1/AE3; therefore, the primary site of the tumor was not the thymus. In addition, the macroscopic findings in our current case were similar to those of metastatic lymphoma in the upper mediastinum lymph node in a lymphoma cell-injected mouse model reported by Matsumoto *et al*[17]. In general, B-cell lymphomas in mice typically occur in the spleen, mesenteric lymph node, and Peyer's patches; therefore, B-cell lymphomas arising from cranial mediastinal lymph nodes are uncommon[10, 11, 15].

In conclusion, we describe a case of spontaneous B-

cell lymphoma in the cranial mediastinal lymph node of an aged male C57BL/6J mouse. B-cell lymphoma in the cranial mediastinal lymph node is rarely observed. To the best of our knowledge, this case report is the first to document the occurrence of B-cell lymphoma in the cranial mediastinal lymph node of an aged male mouse of this strain.

Disclosure of Potential Conflicts of Interest: The authors declare that they have no conflict of interest.

Acknowledgments: We would like to thank Katsuya Fujiki of the Safety Research Laboratories and Sayuka Katou of the Oncology & Immunology Unit of Mitsubishi Tanabe Pharma Corporation for their assistance with this study.

References

1. Son WC, and Gopinath C. Early occurrence of spontaneous tumors in CD-1 mice and Sprague-Dawley rats. Toxicol Pathol. **32**: 371–374. 2004. [Medline] [CrossRef]
2. Haines DC, Chattopadhyay S, and Ward JM. Pathology of aging B6;129 mice. Toxicol Pathol. **29**: 653–661. 2001. [Medline] [CrossRef]
3. Nakamura K, Kuramoto K, Shibasaki K, Shumiya S, and Ohtsubo K. [Age-related incidence of spontaneous tumors in SPF C57BL/6 and BDF1 mice]. Jikken Dobutsu. **41**: 279–285. 1992 (in Japanese). [Medline]
4. Dunn TB. Normal and pathologic anatomy of the reticular tissue in laboratory mice, with a classification and discussion of neoplasms. J Natl Cancer Inst. **14**: 1281–1433. 1954. [Medline]
5. Pattengale PK, and Taylor CR. Experimental models of lymphoproliferative disease. The mouse as a model for human non-Hodgkin's lymphomas and related leukemias. Am J Pathol. **113**: 237–265. 1983. [Medline]
6. Frith CH, Ward JM, and Chandra M. The morphology, immunohistochemistry, and incidence of hematopoietic neoplasms in mice and rats. Toxicol Pathol. **21**: 206–218. 1993. [Medline] [CrossRef]
7. Fredrickson TN, Hartley JW, Morse HC 3rd, Chattopadhyay SK, and Lennert K. Classification of mouse lymphomas. Curr Top Microbiol Immunol. **194**: 109–116. 1995. [Medline]
8. Frith CH, Ward JM, Harleman JH, Stromberg PC, Halm S, Inoue T, and Wright JA. Hematopoietic system. In: International Classification of Rodent Tumors. The Mouse. U Mohr (ed). Springer-Verlag, Berlin Heidelberg. 417–451. 2001.
9. Morse HC 3rd, Anver MR, Fredrickson TN, Haines DC, Harris AW, Harris NL, Jaffe ES, Kogan SC, MacLennan ICM, Pattengale PK, Ward JM. Hematopathology subcommittee of the Mouse Models of Human Cancers Consortium. Bethesda proposals for classification of lymphoid neoplasms in mice. Blood. **100**: 246–258. 2002. [Medline] [CrossRef]
10. Willard-Mack CL, Elmore SA, Hall WC, Harleman J, Kuper CF, Losco P, Rehg JE, Rühl-Fehlert C, Ward JM, Weinstock D, Bradley A, Hosokawa S, Pearse G, Mahler BW, Herbert RA, and Keenan CM. Nonproliferative and proliferative lesions of the rat and mouse hematolymphoid system. Toxicol Pathol. **47**: 665–783. 2019. [Medline] [CrossRef]
11. Ward JM. Lymphomas and leukemias in mice. Exp Toxicol Pathol. **57**: 377–381. 2006. [Medline] [CrossRef]
12. Borowsky AD, Munn RJ, Galvez JJ, Cardiff RD, Ward JM, Morse HC 3rd, Kogan SC, Aldape KD, Louis DN, and Bosenberg MW. Mouse models of human cancers (part 3). Comp Med. **54**: 258–270. 2004. [Medline]
13. Rehg JE, and Sundberg JP. Utility of antiPax5 in the diagnosis of lymphoproliferative disorders and neoplasia in mice. Comp Med. **58**: 246–252. 2008. [Medline]
14. Rehg JE, Rahija R, Bush D, Bradley A, and Ward JM. Immunophenotype of spontaneous hematolymphoid tumors occurring in young and aging female CD-1 mice. [Corrected]. Toxicol Pathol. **43**: 1025–1034. 2015. [Medline] [CrossRef]
15. Shibutani K, Hisada S, Tamura K, Ohmachi Y, and Hosokawa S. Immune system. In: Toxicologic Histopathology. Japanese Society of Toxicologic Pathology (ed). Nishimura Shoten, Tokyo. 445–476. 2017 (in Japanese).
16. Van den Broeck W, Derore A, and Simoens P. Anatomy and nomenclature of murine lymph nodes: descriptive study and nomenclatory standardization in BALB/cAnNCrl mice. J Immunol Methods. **312**: 12–19. 2006. [Medline] [CrossRef]
17. Matsumoto T, Suetsugu A, Shibata Y, Nakamura N, Aoki H, Kunisada T, Tsurumi H, Shimizu M, and Hoffman RM. A color-coded imageable syngeneic mouse model of stromal-cell recruitment by metastatic lymphoma. Anticancer Res. **35**: 4647–4654. 2015. [Medline]